Contents lists available at ScienceDirect

International Journal of Rock Mechanics and Mining Sciences

journal homepage: www.elsevier.com

The effect of thermal cycles on limestone mechanical degradation

C.J. Villarraga[a,*], M. Gasc-Barbier[b], J. Vaunat[a], J. Darrozes[c]

[a] Department of Civil and Environmental Engineering, Technical University of Catalonia (UPC), Campus Nord UPC, Barcelona, Spain
[b] Centre for studies and expertise on risks, environment mobility and urban and country planning (CEREMA), Aix-en-Provence, France
[c] Geoscience Environnement Toulouse, UPS, CNRS, IRD, Université de Toulouse, Toulouse, France

ARTICLE INFO

ABSTRACT

This work presents the results of an experimental program performed to study the effect of long series of moderate thermal cycles on the mechanical response of a limestone rock. Samples were exposed to more than 1000 temperature cycles from 10° to 50°C in dry conditions. Rock degradation was followed by measuring axial and radial strains, elastic wave velocities and uniaxial compression strength during the test. Results evidence an accumulation of strains and a decrease in P-wave velocity and uniaxial compression strength with no noticeable change in porosity. This study highlights the important effects that temperature cycles have on rock mechanical properties, even for moderate cycle amplitudes.

1. Introduction

Rockfall is one of the main component of landscape evolution and there is a variety of geomorphological factors that contribute to their occurrence. Rock massif structural features, toe erosion, rainfall, earthquake, freeze-thaw cycles, weathering and meteorization or tectonic induced deformations are the most common factors identified as controlling this hazard.[1–10] Another mechanism sometimes pointed out is the slow degradation of rock mechanical properties and the resulting progressive accumulation of displacements under thermal cycles in the climatic range. Cases that typify this mechanism, which may lead to the failure of the rock massif without any evident external triggering factors have been presented by many authors.[7–10]

Under cyclic changes in temperature, rock massifs experience expansion/contraction cycles that cause continuous stress redistribution in the zone of propagation and retrieval of the heat front. Because the amplitudes of temperature changes under climatic actions are moderate and it is generally considered that their maximum and minimum values were already reached during rock slope history, stress changes are in most cases expected to produce recoverable deformations. This is however not the case when there is a change in rock slope conditions, either because of weathering, exposure of new rock faces after failure or climate change. In the last two cases, points inside the massif may experience previously unreached levels of temperature-induced stress and deformations, which could reactivate existing discontinuities or create and propagate new ones.[2,5,6,11] Hall and Thorn[2] analyzed the rate of temperature increase able to generate stress reaching the failure criterion at the heat front and propose to consider 1 °C/min as a typical rate.

A different aspect is the low accumulation of deformation under change of stress at levels far for failure. This phenomenon, identified in others materials as ratchetting or fatigue, is generally related to micro-slips and rearrangement at grains level. In rocks under thermal load, it is often considered that the differential of thermal expansion between the minerals constituting the rock makes increases the intensity of stress at grains contact, which in turn furthers decohesion and microcracking. This mechanism is mostly influenced by grain arrangement and thermal expansion coefficient.[11–14] It may be at the source of degradation of rock mechanical properties like elastic moduli,[15] tensile strength,[16] or uniaxial compression strength.[14,16,17] For example, Cheng et al.[17] presented results obtained on granite samples subjected to thermal cycles between − 20 °C and 65 °C, and found 30% decrease in the uniaxial compression strength value after 40 thermal cycles. Evolution of material damage under thermal cycles is generally monitored by looking at the variation of elastic wave velocity, because of the non-intrusive character of the method and the strong sensitivity of the parameters on the presence and development of defaults in the material.[15,18–22]

This technical note aims at contributing to this last issue by implementing a laboratory experimental research to evaluate the response of

* Corresponding author.
Email address: claudia.juliana.villarraga@upc.edu (C.J. Villarraga)

https://doi.org/10.1016/j.ijrmms.2018.06.017
Received 14 November 2017; Received in revised form 16 June 2018; Accepted 25 June 2018
Available online xxx
1365-1609/

limestone rock samples under long series of temperature cycles in the range of climatic variations (10–50 °C).

2. Experimental layout

The experimental program has been carried out on cylindrical samples obtained from a calcareous rock slope at La Roque Gageac (LaRG), France. The cliff is constituted by layers of marine limestone dating from the intermediate and upper Coniancian[23–25] and having suffered a strong karstification process. As a matter of fact about the rock hardness, the mean value of uniaxial compression strength obtained in previous studies is equal to 47.4 MPa with a standard deviation of 9.63 MPa. This fact highlights the high heterogeneity of the material.

Samples were retrieved from two distinct places: from blocks inside a troglodyte cavern (i.e. essentially protected from solar radiation) and cores drilled from the face of the cliff. Drilling was performed in two directions: horizontally (perpendicular to the cliff) and vertically (perpendicular to a horizontal natural platform present in the cliff). As cliff stratification is almost horizontal, samples drilled horizontally are parallel to the stratification planes while vertical samples are perpendicular to it.

Table 1 shows the thermal and physical properties of LaRG's limestone taken for previous studies. Material has in average a porosity equal to 17% whose about 6% is captured inside grains and do not participate to the connected porous network. The thermal expansion coefficient obtained in the laboratory and by back-analysis of field deformations under climatic change in temperature is between 3×10^{-6} and 6×10^{-6} °C^{-1}.

Table 1
Physical properties of LARG limestone.

Density ρ	2382 kg/m^3
Total porosity n_t	17.0%
Connected porosity n_c	11.2%
Water ratio, w	4.7%
Thermal expansion coefficient	6 (+/− 3). 10^{-6} °C^{-1}.

Test procedure was as follows: after mineralogical analysis, each sample was installed in a climatic chamber and tested under a target number of thermal cycles. Deformation and elastic wave propagation velocities were followed during the test. For some tests, samples have been retrieved from the climatic chamber after a given number of cycles (see Table 2) and the uniaxial compression strength determined in order to estimate its degradation.

Table 2 presents the characteristics of the different samples at the beginning of each test. Porosity has been calculated from the dry and solid density of the samples measured in laboratory. Solid density for block samples is equal to 2.72 g/cm^3 and to 2.76 g/cm^3 for samples directly drilled from the face of the cliff. They show very narrow values due to the fact that the density of the minerals composing the rock is quite similar.

Samples obtained from blocks are characterized by an initial mean value of P-wave velocity equal to 4400 m/s, while the mean value for samples drilled from the cliff is 2920 m/s. This variation may be due to both differences in porosity and rock stiffness.

2.1. Samples mineralogy

Mineralogy of the samples has been determined by Infrared spectrometry (IRA) tests (see Fig. 1). Samples obtained from the blocks exhibit a typical calcite spectrum,[26–28] whereas the spectrum for samples from the cliff face is difficult to interpret. Complementary X-Ray Diffraction (XRD) test showed that they are composed of two phases (calcite and quartz) with a weight fraction equal to approximately 50–50% (Fig. 2).

Table 2
Samples characteristics at the beginning of the tests. Vp, Vs, DEF and UCS denote P-wave velocity, S-wave velocity, deformation and Uniaxial Compression Strength, respectively. B, CH and CV denote samples obtained from blocks and cores drilled vertically and horizontally from the cliff face, respectively.

Sample	*Vp* (m/s)	Mineralogy	Porosity (%)	Number of cycles	*Def*	*Vp - Vs*	*UCS*
B1	4347	Calcite	15.86	948	X		
B2	4637	Calcite	10.13	948	X	X	
B3	4480	Calcite	11.75	948	X	X	
B4	4252	Calcite	15.91	Measure of temperature inside the sample			
B5	4342	Calcite	15.47	828		X	X
B6	4282	Calcite	16.29	828		X	X
B7	4177	Calcite	17.49	828		X	X
B8	4407	Calcite	15.38	624			X
B9	4404	Calcite	15.29	624			X
B10	4321	Calcite	13.52	624			X
B11	4373	Calcite	14.73	420			X
B12	4402	Calcite	14.80	420			X
B13	4485	Calcite	13.88	420			X
B14	4486	Calcite	14.29	210			X
B15	4389	Calcite	14.13	210			X
B16	4441	Calcite	13.29	210			X
B17	4381	Calcite	13.95	0			X
B18	4483	Calcite	13.45	0			X
B19	4380	Calcite	14.56	0			X
CV1	3165	Calcite-Quartz	18.50	910	X	X	
CV2	2831	Calcite-Quartz	20.87	1222		X	
CV3	2517	Calcite-Quartz	18.91	1222		X	
CV4	2831	Calcite-Quartz	20.76	910	X	X	
CV5	2727	Calcite-Quartz	19.91	1222		X	
CH1	3027	Calcite-Quartz	18.29	1222		X	
CH2	3039	Calcite-Quartz	17.93	910	X	X	
CH3	3348	Calcite-Quartz	17.46	1222		X	
CH4	2880	Calcite-Quartz	20.03	1222		X	
CH5	2829	Calcite-Quartz	20.70	910	X	X	

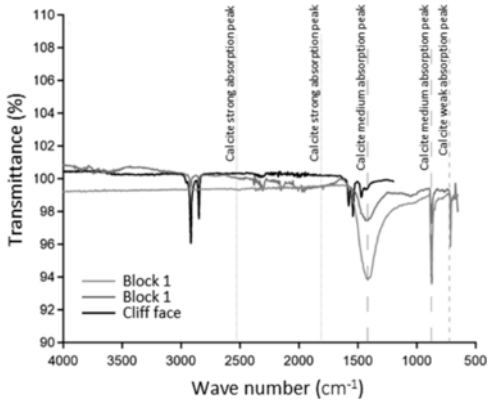

Fig. 1. Infrared spectra of calcite samples (Block 1 and Block 2) and quartz-calcite samples (Cliff face) compared with typical calcite peaks.

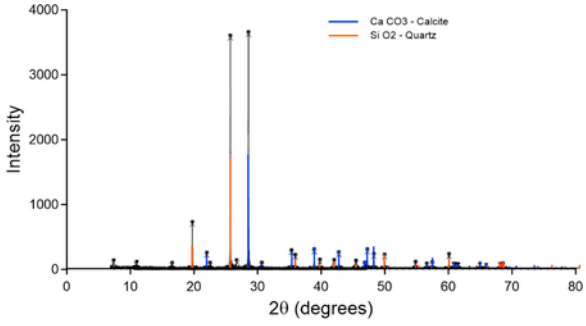

Fig. 2. XRD analysis of samples drilled from the face of the cliff.

Fig. 3 shows micrographs of thin sections cut from different samples. They show important mineralogical differences between samples obtained from the blocks and the cliff, which confirms the results from the IRA and XRD analyses. Samples obtained from blocks are mainly composed of calcite with two types of crystallinity: (i) micrite, darker and without clear crystalline shape and (ii) sparite, which corresponds to the lighter part with a coarse crystalline shape. A low portion of quartz (colorless minerals with low positive relief in natural light) is also observed. Thin sections obtained from the cliff face also show calcite minerals in both type of textures, sparite and micrite. However, an important percentage of voids are observed in the thin section (light grey/light pink zones). It is assumed that these voids correspond to quartz minerals identified by XRD analyses and lost during the preparation of the sample.

2.2. Application of heating-cooling cycle

Thermal cycles were imposed by placing the samples inside a climatic chamber. The temperature of each thermal cycle vary from 10 °C to 50 °C, which corresponds to typical climatic temperature variations. In order to reach temperature equilibrium within the samples, each heating/cooling ramp was applied during 1 h. Equilibrium was verified by measuring temperature inside one test probe.

The temperature variation rate has been targeted to 0.35 °C/min in order to remain far from the rate of 1 °C/min defined by Hall and Thorn.[2]

2.3. Measurement of deformation

Axial and radial deformation were measured by strain gauges glued on each sample in vertical and horizontal direction. Because the strain gauges are submitted to thermal variations, they were set in a half-bridge circuit with thermal compensation. Deformation measurements were registered using a five minutes sampling frequency during the whole tests.

2.4. Measurement of elastic wave velocities

Wave propagation velocities were measured during the tests using the ultrasonic pulse technique according to French standard NF P 94–411.[29] Compression waves (P-waves) and shear waves (S-waves) in two perpendicular directions (S1 and S2) are induced by an electric pulse generator that produces waves over 250 V for a maximum rise duration of 0.2 ms. This generator is connected to transmitter/ receptor transducers with a resonance frequency from 25 kHz to 1 MHz. The sample is fixed between transmitter/receptor transducers in a frame provided with a uniaxial pump, to assure good contact between the sample and the transducers, without applying mechanical load to the sample. A force transducer is used to control that the applied load is 2 kN. To have a proper wave transmission between the sample and the transducers, very thin sheets of lead are fixed with honey on the transducers face. Finally, the signals are registered by a 10 ns-time resolution oscilloscope connected to a personal computer. All the devices were installed in a temperature controlled room.

The bulk density of the sample ρ and the elastic wave propagation velocity measurements (V_p and V_s) can be used to calculate the dynamic Young modulus (E) and the dynamic Poisson ratio (ν), as follows:[15]

$$E = \rho \frac{V_s^2(3V_p^2 - 4V_s^2)}{(V_p^2 - V_s^2)} \quad (1)$$

$$\nu = \frac{(V_p^2 - 2V_s^2)}{2(V_p^2 - V_s^2)} \quad (2)$$

2.5. Measurement of uniaxial compressive strength

Finally, in order to evaluate the effect of thermal cycling on the mechanical response of the material, uniaxial compression tests were performed on samples obtained from the blocks. Experimental procedure followed the ASTM D7012-10 standard.[30] Young modulus was determined as the mean slope of the strain-stress curve during unloading/loading cycles realized at 50% and 80% of the reference uniaxial compression strength, previously estimated (47.3 MPa). The loading/unloading rate was set at 0.15 MPa/s. As the tests focus on the determination of elastic moduli variation rather than absolute value, it has been chosen to measure the axial deformation externally by LVDTs.

Fifteen cylindrical samples were tested in the uniaxial compression device. They were divided in five groups, each one subjected to a given number of cycles: 0, 210, 420, 624 and 828. Each group is composed by three samples: one from block and two from horizontal and vertical cliff cores, respectively. P-wave velocity was measured on each sample before and after the compression test.

3. Experimental results

3.1. Deformations

Fig. 4 presents the evolution of the radial and axial deformations measured during cycles application on block samples B1 and B3 and on

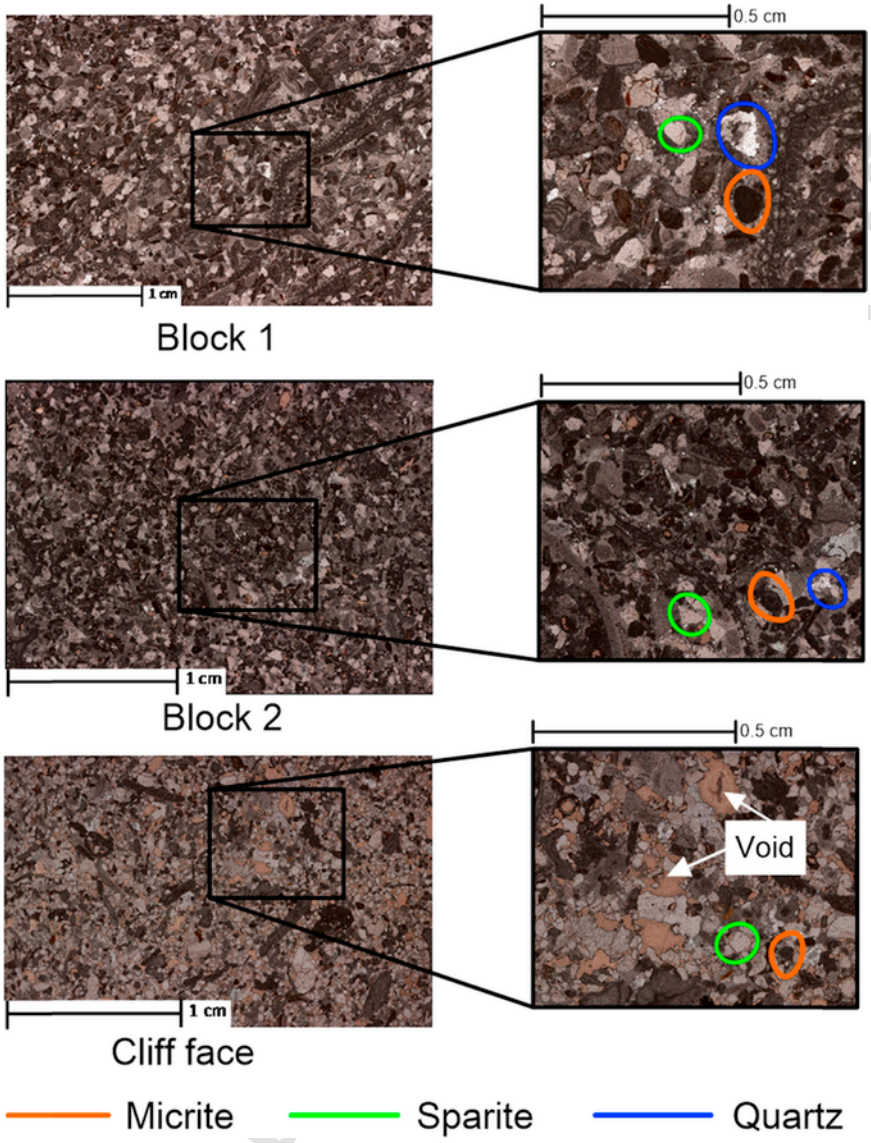

Fig. 3. Micrographs of thin sections obtained on block and cliff samples.

core samples CV4 and CH2. The Rock Mechanics convention is used (positive strain means extension). In all the cases, an accumulation of deformation can be observed as the number of cycles increase. Accumulation is in extension for samples B1, B3 and CV4 and seems to stabilize consistently around value close to 3×10^{-4} and 6×10^{-4} for the axial and radial strain, respectively. However, sample CH2 accumulates compressive strains during the cycles with quite a high value for the axial strain (2.2×10^{-3}). This fact can be related to the loss of P-wave velocity registered for the four cases. For samples B3 and CV4, P-wave variation is less than 1% and 5%, respectively, while it increases to 10% for sample CH2. It is thus possible that samples B1, B3 and CV4 experience microstructural rearrangement during thermal expansion/contraction that traduces in a global expansion of the sample and the consequent decrease in P-wave velocity, while sample CH2 suffers a higher damage that degrade the material and traduces into an overall compression.

Further inside into the evolution of material deformation is presented in Fig. 5 by plotting the loop of strain against temperature for different cycle numbers: 50th, 100th, 500th and 900th. Plots present essentially closed hysteric loops that shift with the number of cycles. Material thermal expansion coefficient $\alpha_{h,v} = \Delta\varepsilon_{h,v} / \Delta T$ can be assessed for each loop and each strain component as the mean slope of the hysteretic loop. Values obtained for the four samples are compiled in Table 3. They indicate values between 3×10^{-6} and 1×10^{-5}, which are consistent with values obtained in previous studies, either in the laboratory or by back-analysis of field measurements.[31] There is moreover no variation between the thermal expansion coefficient and the number of cycles.

Shift in hysteretic loop is directly related to the accumulation of strain shown in Fig. 4. It is interesting to note that there is no discernable accumulation of strain during one cycle. Some hysteresis can be observed in the different strain loops. It could be a genuine effect of temperature gradient on material mechanical response, or simply due to the delay in temperature change caused by material heat storage during heating/cooling reversal (as in any diffusive process). In any case, effect is general small and does not change much with the number of cycles. Exceptions are the last loop in radial strain for sample B3 and the first two loops in axial strain for samples CH2, but data are two scarce to draw conclusions from these data.

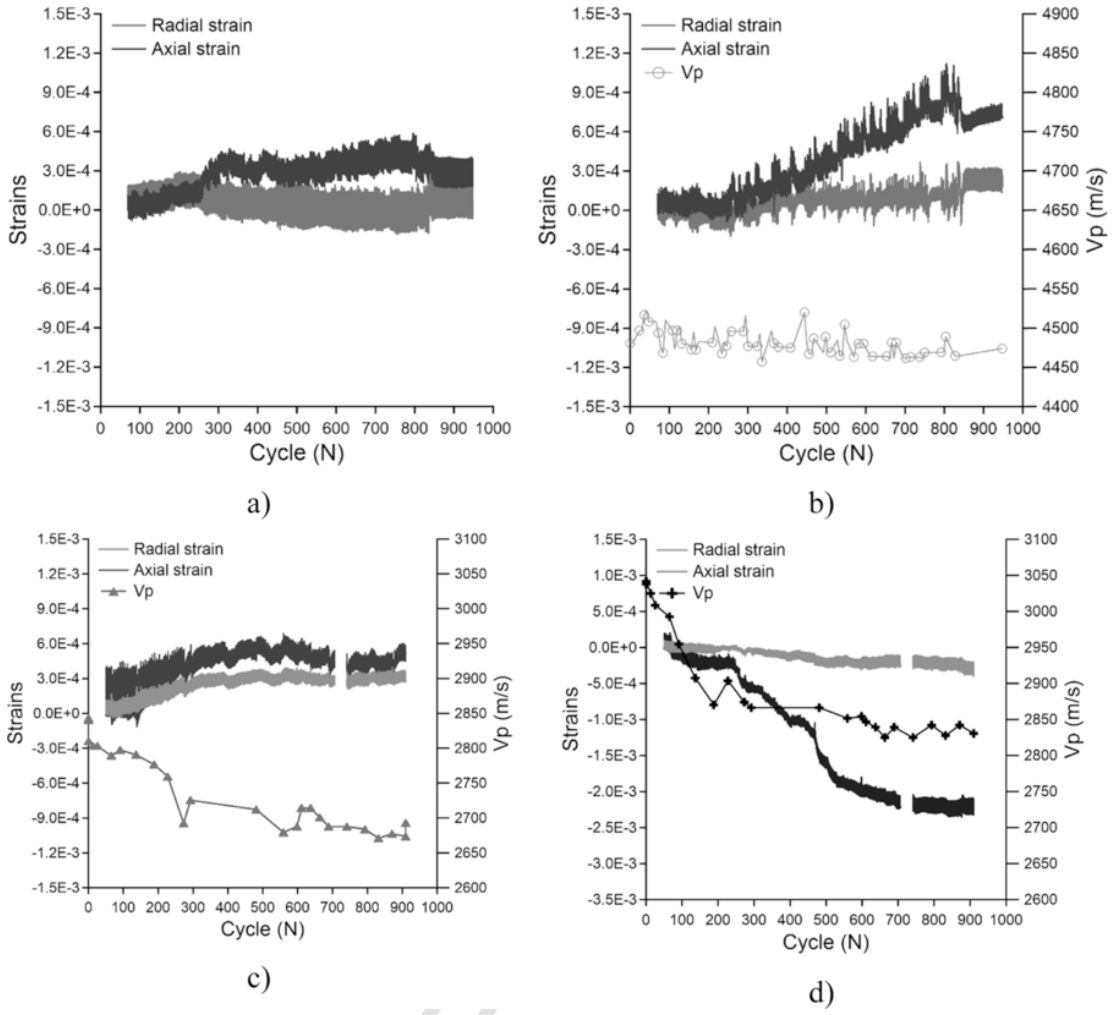

Fig. 4. Evolution of P-wave velocity and strains during thermal cycles for samples: a) B1; b) B3; c) CV4; and d) CH2.

3.2. Elastic wave propagation velocity

Table 4 compiles the initial values in P-wave velocity as well as its decrease at the end of the heating test, all the samples subjected to more than 900 temperature cycles. Decrease of S-wave velocity and in corresponding Young's moduli are also presented in the table for the same samples.

Initial P-wave velocities for sample B2, B3, B5, B6 and B7 (extracted from the blocks) are between 4200 and 4600 m/s. These values are much higher than the ones measured on CV and CH samples (typically between 2500 and 3100 m/s). This difference can be explained by two facts. On the one hand, B-samples are essentially made of calcite while the C-samples are composed by both calcite and quartz. On the other hand, the C samples, extracted from the face of the cliff are more degraded as they known higher temperatures due to direct solar radiation while B-samples, located inside the troglodyte cavern, experience only changes in temperature due to changes in air temperature. This interpretation can be partly confirmed by the fact that sample CH3, located at 30 cm from cliff face, has a higher P-wave velocity than sample CH2 and CH1, located at 18 and 6 cm for cliff face, respectively, and thus in a more weathered zone.

Fig. 6 depicts the evolution of P-wave velocity with temperature cycles for all the three samples drilled horizontally in the cliff. They all experience a decrease in P-wave velocity of about between 11% and 12% after 900 cycles. This result is consistent with the fact that all the samples have a similar mineralogy and porosity (18.29%, 17.93% and 17.46%, respectively). Moreover, values of total decrease in Young's modulus (computed from P- and S-wave velocities) presented in Table 4 for CH4 and CH5 indicate that the loss in stiffness tends to increase for samples with higher porosity (13.2% and 14.9% for porosities equal to 20.03% and 20.7%, respectively). A similar trend is observed for block samples, for which the loss of Young's modulus passes from 2% to 7.1% when the porosity increases from 10.13% to 17.49%. Conversely, no conclusions between rock elastic degradation and porosity can be drawn for CV-samples.

Fig. 7a presents a comparison of the decrease in Young's modulus (computed from P- and S-wave velocities) obtained in B-, CH- and CV- samples. B3 and B6 samples exhibit a lower moduli degradation (2.0% and 4.7%, respectively) than CV4 (6.4%) and CH2 (11%) samples. This results can be interpreted again as due to the different mineralogies and porosities. B3 sample, which suffers the lowest degradation, is composed by essentially one phase material and have a low porosity (11.75%). B6 has a level of porosity close to the one of CH3, but suffered less degradation because it is composed only by calcite. Samples composed by two minerals – quartz and calcite – suffered the highest degradation. Differential thermal expansion between mineral grains can thus be one the factor enhancing rock damage.

A strategy to assess the damage of the sample is to compute the Fracturation Degree Index, defined as:[32,33]

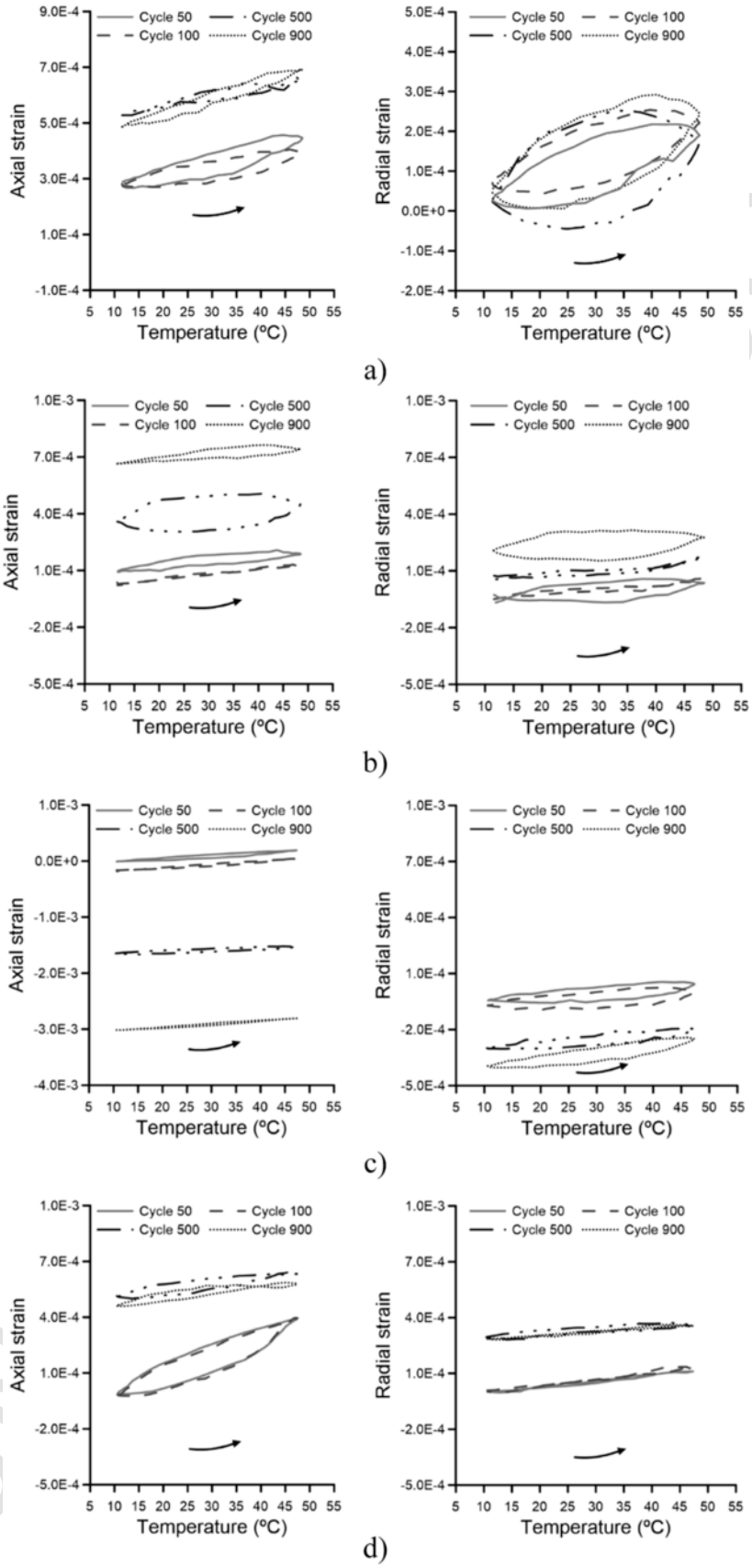

Fig. 5. Plots of axial and radial strain vs temperature for thermal cycles 50, 100, 500 and 900 and for samples: a) B1; b) B3; c) CV4; and d) CH2.

Table 3
Thermal expansion coefficients computed from strain measurements for distinct temperature cycles.

	Sample B 1		Sample B 3		Sample CV 4		Sample CH 2	
Cycle	Vertical ($°C^{-1}$)	Radial ($°C^{-1}$)	Vertical ($°C^{-1}$)	Radial ($°C^{-1}$)	Vertical ($°C^{-1}$)	Radial ($°C^{-1}$)	Vertical ($°C^{-1}$)	Radial ($°C^{-1}$)
50	4.0e − 6	4.0e − 6	3.0e − 6	2.0e − 6	1.0e − 5	2.0e − 6	7.0e − 6	2.0e − 6
100	3.0e − 6	3.0e − 6	3.0e − 6	3.0e − 6	1.0e − 5	4.0e − 6	6.0e − 6	2.0e − 6
500	3.0e − 6	4.0e − 6	2.0e − 6	3.0e − 6	3.0e − 6	2.0e − 6	3.0e − 6	3.0e − 6
900	6.0e − 6	5.0e − 6	2.0e − 6	2.0e − 6	3.0e − 6	2.0e − 6	6.0e − 6	4.0e − 6
mean	4.0e − 6	4.0e − 6	2.5e − 6	2.5e − 6	6.5e − 6	2.5e − 6	5.5e − 6	2.7e − 6

Table 4
Change in elastic wave propagation velocities and elastic moduli after 900 cycles of thermal load.

Sample	Initial *Vp* (m/s)	Decrease in *Vp* (%)	Decrease in *Vs* (%)	Decrease in Young's modulus (%)
B 2	4637	1.4	2.6	2.0
B 3	4480	0.1	0.3	1.3
B 5	4342	4.0	2.5	5.3
B 6	4282	2.9	1.7	4.7
B 7	4177	3.8	3.2	7.1
CV 1	3165	6.8	3.9	10.6
CV 2	2831	14.0	11.7	23.4
CV 3	2517	8.1	9.5	17.1
CV 4	2831	5.2	2.5	6.4
CV 5	2727	14.3	10.0	33.9
CH 1	3027	7.0	6.5	11.5
CH 2	3039	7.0	4.8	11.0
CH 3	3348	9.0	4.7	12.2
CH 4	2880	6.6	7.8	13.2
CH 5	2829	6.4	8.7	14.9

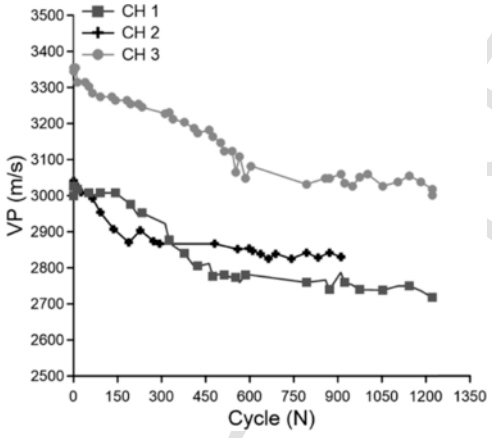

Fig. 6. Evolution of P-wave velocity with number of cycles for samples CH1 to CH3.

$$\mathrm{DF} = 1 - \frac{IC}{1 - 1.4\phi} \tag{3}$$

where $IC = V_p/V_p^*$ is called the continuity index, ϕ is the porosity, and V_p^* is the P-wave velocity of the pure mineral. For intact one-mineral material, IC has been found to be approximately equal to $1 - 1.4\phi$. DF is thus supposed to give the part of the voids that are only due to cracks and allows to compare their evolution for samples that don't have the same mineralogy.

Fig. 7b shows the evolution of DF during the heating/cooling cycles for samples B3, B6, CV4 and CH2. V_p^* has been taken equal to 6660 m/s for the block samples and to 6355 m/s for cliff samples. Samples B3 and B6 present lower initial fracturing degrees than samples CH2 and CV4, which can be related to a lower number of cracks in the samples. In the same way, samples obtained from the cliff face (CH2 and CV4) present an important increase of fracturing degree with thermal cycles, suggesting that micro-fissure develop in the material during the thermal load.

3.3. Uniaxial compressive strength

Uniaxial Compression tests have been performed on block samples previously subjected to different number of cycles. Fig. 8 depicts the axial stress vs axial strain obtained for five specimens after 0, 210, 420, 624 and 828 cycles, respectively. Data evidence a decrease in the peak value (*UCS*) and in the slope of the pre-peak curve (moduli). They also show an increase in the peak strain and of the strain for which material starts to exhibit stiffness, often associated to the stage at which material open fissures are closed by loading. After the peak, the change in the strain-stress curve is less evident but seems to evidence a less brittle response. All these results consistently indicate a degradation of the material, which becomes softer and more ductile.

Fig. 9a shows the evolution of the UCS and of the initial Young's modulus (computed from the P- and S-wave velocity measured before the start of the compression test) with the number of cycles. Both parameters experience a similar decrease with heating/cooling cycles. This is confirmed by the relationship existing between the UCS and the P-wave velocity at the beginning of the compression test. Both variables appear to be strongly correlated by a potential relation similar to the one proposed by Najibi et al.[34]:

$$\sigma_c = 1.891 \mathrm{Vp}^{2.152} \tag{4}$$

with a correlation coefficient of $R^2 = 0.8308$ (see Fig. 9b). This confirms that P-wave velocity is a good parameter to evaluate rock damage both in terms of elastic moduli and strength.

4. Concluding remarks

An experimental program has been developed to evaluate thermal damage on rocks under long series of temperature cycles in the range of climatic actions (between 10º and 50 °C). Results from the experiments evidence accumulation of deformations and degradation of mechanical properties under the applied thermal cyclic load.

Measurements of P- and S- wave velocities evidence a decrease in both elastic wave velocities during the thermal cyclic load. After more than 900 cycles, decrease is typically above 10% for calcite-quartz

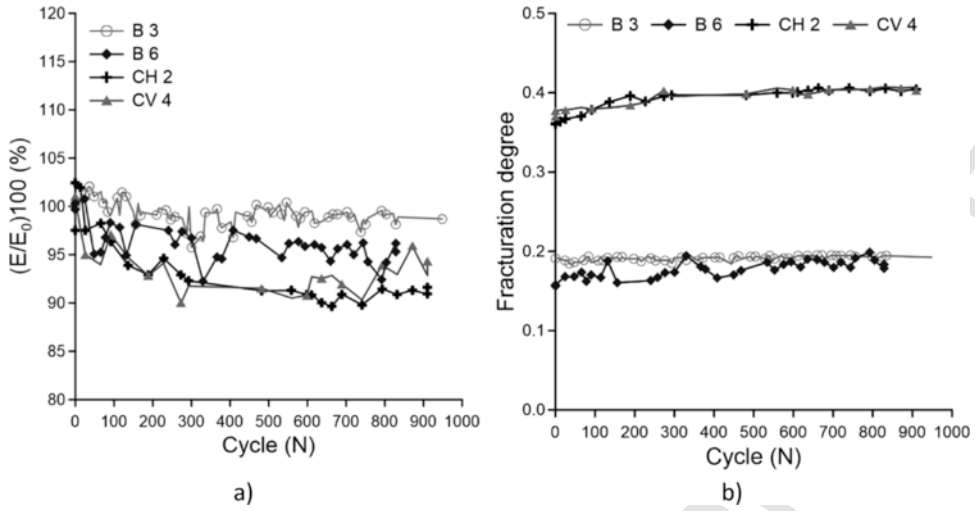

Fig. 7. Evolution of samples damage variables with thermal cycles: a) degree of damage; b) fracturation degree index.

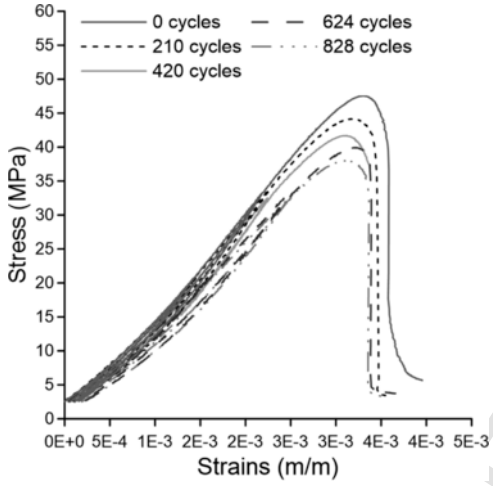

Fig. 8. Strain-stress curves obtained during uniaxial compression tests performed on samples previously damaged under different numbers of cycles (B18: 0 cycles; B15: 210 cycles; B12: 420 cycles; B9: 624 cycles and B5: 828 cycles).

samples and around 5% for pure calcite samples. Similar evidences have been presented by.[4,21,22,35,36].

Decrease in strength is also observed during thermal cycling. Percentage of degradation is of the same order as for the elastic wave velocity, indicating that the process of damage at moderate temperature seems to have a similar effect on elastic and strength properties. Moreover, a strong correlation has been observed between the UCS and the P-wave velocity for all the cycles.

Visual observations do not evidence the development of fissure or fracture across the sample, indicating that the damage is essentially due to processes acting at the micro-scale. Fig. 10 shows moreover Mercury Intrusion Porosimetry tests that highlight no significant change in material Pore Size Distribution during heating. Particularly, the one-mode distribution remains unchanged during cycles application, indicating heating does not generate new voids in the material. As a consequence, it can be reasonably considered that the rock degradation is essentially due to the generation or propagation of internal micro-cracks. This mechanism is consistent with the one proposed by,[2,37] who estimated that these features essentially develop at grains contacts.

Comparison between P-wave velocities of quartz-calcite samples extracted from the cliff face show that deeper samples have a higher P-wave velocity, although having similar values of porosity. This is consistent with the existence of a zone of rock degradation due to climatic actions, whose intensity decreases for points located farther for

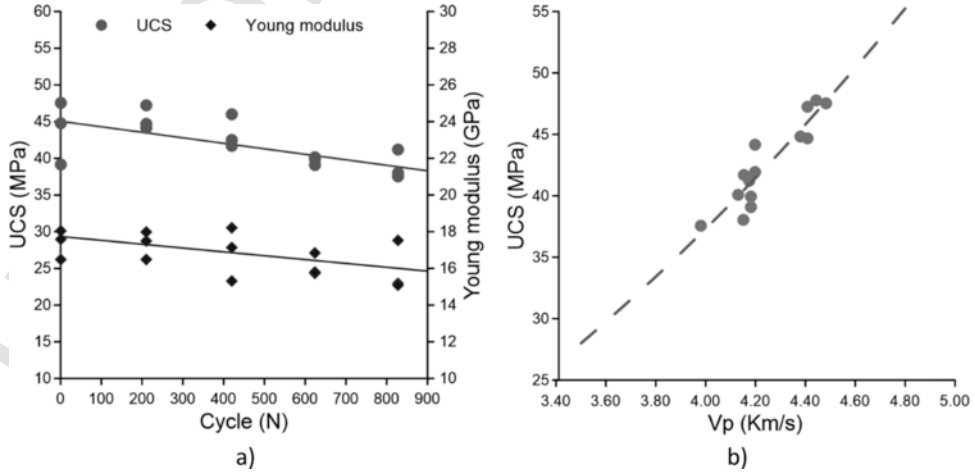

Fig. 9. Comparison between rates of damage for strength and elastic parameters: a) evolution of UCS and Young's modulus during thermal cycles; b) variation of UCS vs P-wave velocity.

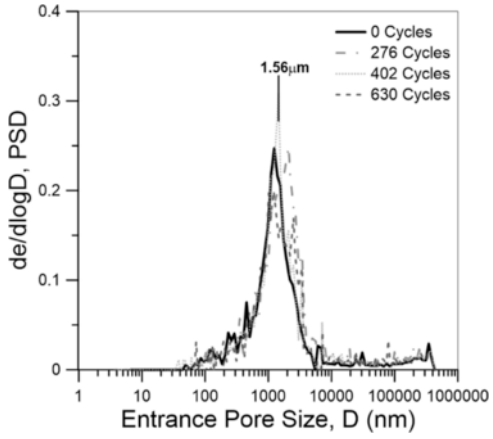

Fig. 10. Pore size distribution obtained on block samples after 0, 276, 402 and 630 thermal cycles.

the rock-atmosphere interface. This is confirmed by the fact that points with higher P-wave velocity also experiment the highest degradation under the thermal cycles applied in the laboratory, which would indicate that they are initially in a more intact state.

Pure calcite samples evidence more damage when the porosity is higher. On the other hand, they exhibit less degradation than calcite-quartz samples for similar values of porosity. This can be attributed to two effects: the higher stiffness of the calcite and the fact that there is no differential thermal expansion as there is essentially one mineral phase.

Acknowledgments

The authors gratefully acknowledge D. Virely, V. Gendre, J.C. Mercadal, and P. Baro from the CEREMA Toulouse, France, the staff from the laboratory GET of the Université Paul Sabatier, Toulouse, France and A. Pereve from CEREMA Aix-en-Provence, France, for their valuable support in the laboratory work.

References

1. M. Julian, E. Anthony, Aspects of landslide activity in the Mercantour Massif and the French Riviera, southeastern France, Geomorphology 15 (3–4) (1996) 275–289, https://doi.org/10.1016/0169-555X(95)00075-G.
2. K. Hall, C.E. Thorn, Thermal fatigue and thermal shock in bedrock: an attempt to unravel the geomorphic processes and products, Geomorphology 206 (2014) 1–13, https://doi.org/10.1016/j.geomorph.2013.09.022.
3. N. Matsuoka, H. Sakai, Rockfall activity from an alpine cliff during thawing periods, Geomorphology 28 (3–4) (1999) 309–328, https://doi.org/10.1016/S0169-555X(98)00116-0.
4. H. Yavuz, Effect of freeze-thaw and thermal shock weathering on the physical and mechanical properties of an andesite stone, Bull Eng Geol Environ 70 (2) (2011) 187–192, https://doi.org/10.1007/s10064-010-0302-2.
5. D. Bakun-Mazor, Y.H. Hatzor, S.D. Glaser, J. Carlos Santamarina, Thermally vs. seismically induced block displacements in Masada rock slopes, Int J Rock Mech Min Sci 61 (2013) 196–211, https://doi.org/10.1016/j.ijrmms.2013.03.005.
6. B.D. Collins, G.M. Stock, Rockfall triggering by cyclic thermal stressing of exfoliation fractures, Nat Geosci (2016) 1–7, https://doi.org/10.1038/ngeo2686.
7. C. Clément, V. Merrien-Soukatchoff, C. Dünner, Y. Gunzburger, Stress measurement by overcoring at shallow depths in a rock slope: the scattering of input data and results, Rock Mech Rock Eng 42 (4) (2009) 585–609, https://doi.org/10.1007/s00603-008-0019-8.
8. V. Merrien-Soukatchoff, C. Clément, Y. Gunzburger, Thermal effects on rock slopes: case study of the "rochers de Valabres" slope (France), ISRM 2007, Specialized Sessions on Rockfall-Mechanism and Hazard Assessment, 2007.
9. E. Do Amaral Vargas, R.Q. Velloso, L.E. Chávez, L. Gusmão, C.P. Do Amaral, On the effect of thermally induced stresses in failures of some rock slopes in Rio de Janeiro, Brazil, Rock Mech Rock Eng 46 (1) (2013) 123–134, https://doi.org/10.1007/s00603-012-0247-9.
10. J. Vlcko, V. Greif, V. Grof, M. Jezny, L. Petro, M. Brcek, Rock displacement and thermal expansion study at historic heritage sites in Slovakia, Environ Geol 58 (8) (2009) 1727–1740, https://doi.org/10.1007/s00254-008-1672-7.
11. S. Siegesmund, K. Ullemeyer, T. Weiss, E.K. Tschegg, Physical weathering of marbles caused by anisotropic thermal expansion, Int J Earth Sci 89 (1) (2000) 170–182, https://doi.org/10.1007/s005310050324.
12. K. Hall, The role of thermal stress fatigue in the breakdown of rock in cold regions, Geomorphology 31 (1999) 47–63, https://doi.org/10.1016/S0169-555X(99)00072-0.
13. S.D.C. Walsh, I.N. Lomov, Micromechanical modeling of thermal spallation in granitic rock, Int J Heat Mass Transf 65 (2013) 366–373, https://doi.org/10.1016/j.ijheatmasstransfer.2013.05.043.
14. E. Franzoni, E. Sassoni, G.W. Scherer, S. Naidu, Artificial weathering of stone by heating, J Cult Herit 14 (3 SUPPL) (2013) e85–e93, https://doi.org/10.1016/j.culher.2012.11.026.
15. J.C. Jaeger, N.G.W. Cook, R.W. Zimmerman, Fundamentals of Rock Mechanics, 4th ed., Wiley-Blackwell, Oxford, 2007.
16. Y. Mahmutoglu, Mechanical behaviour of cyclically heated fine grained rock, Rock Mech Rock Eng 31 (3) (1998) 169–179, https://doi.org/10.1007/s006030050017.
17. Y.L. Chen, J. Ni, L.H. Jiang, M.L. Liu, P. Wang, R. Azzam, Experimental study on mechanical properties of granite after freeze-thaw cycling, Environ Earth Sci 71 (8) (2014) 3349–3354, https://doi.org/10.1007/s12665-013-2725-0.
18. A. Luque, E. Ruiz-Agudo, G. Cultrone, et al., Direct observation of microcrack development in marble caused by thermal weathering, Environ Earth Sci 62 (7) (2011) 1375–1386, https://doi.org/10.1007/s12665-010-0624-1.
19. H. Yavuz, R. Altindag, S. Sarac, I. Ugur, N. Sengun, Estimating the index properties of deteriorated carbonate rocks due to freeze-thaw and thermal shock weathering, Int J Rock Mech Min Sci 43 (5) (2006) 767–775, https://doi.org/10.1016/j.ijrmms.2005.12.004.
20. K. Malaga-Starzec, U. Åkesson, J.E. Lindqvist, B. Schouenborg, Microscopic and macroscopic characterization of the porosity of marble as a function of temperature and impregnation, Constr Build Mater 20 (10) (2006) 939–947, https://doi.org/10.1016/j.conbuildmat.2005.06.016.
21. H. Yavuz, S. Demirdag, S. Caran, Thermal effect on the physical properties of carbonate rocks, Int J Rock Mech Min Sci 47 (1) (2010) 94–103, https://doi.org/10.1016/j.ijrmms.2009.09.014.
22. J. Martínez-martínez, D. Benavente, M.A. García-del-cura, Spatial attenuation: the most sensitive ultrasonic parameter for detecting petrographic features and decay processes in carbonate rocks, Eng Geol 119 (3–4) (2011) 84–95, https://doi.org/10.1016/j.enggeo.2011.02.002.
23. Virely D, Guittard J. (2010). *Project DOSMS*: *La Roque Gageac Contexte Géographique, Géologique et Géomécanique Fascicule 2* .
24. PLatel JP. (1987). *Le crétacé supérieur de la plate-forme septentrionale du basin d'Aquitaine Stratigraphie et évolution géodynamique. PhD Thesis*. Université Bordeaux Montaigne.
25. Rey J, Cubaynes R, Fauré P, Hantzpeoue P, Pelissié T. (1988). *Stratigraphie séquentielle et évolution d ' une plate-forme carbonatée*: le Jurassique du. Acad Sci Paris, t360, série II. (February):1009–1015.
26. C.K. Huang, P.F. Kerr, The infrared study of the carbonate minerals, Am Mineral 45 (1960) 311–324.
27. T. Vazquez-Moreno, M.T. BLanco-Varela, Tabla de frecuencias y relacionados con la química del cemento, Mater Constr 31 (182) (1981) 31–48.
28. S. Gunasekaran, G. Anbalagan, S. Pandi, Raman and infrared spectra of carbonates of calcite structure, J Raman Spectrosc 37 (9) (2006) 892–899, https://doi.org/10.1002/jrs.1518.
29. AFNOR. (2002). *Détermination de la vitesse de propagation des ondes ultrasonores en laboratoire*. AFNOR. (NF P 94-411):1-7.
30. ASTM. Standard test method for compressive strength and elastic moduli of intact rock core specimens under varying states of stress and temperatures. D7012-10. 2010;(C):1-8. doi: 10.1520/D7012-13.1.
31. Ruiz D. (2013). *Thermo-mechanical analysis of the stability of a rock-cliff under climatic actions*. upcommons.upc.edu.
32. A. Denis, M. Panet, C. Tourenq, Rock identification by means of continuity index, 4th International Congress on Rock Mechanics, Montreux, Switzerland, 1979125.
33. N. Klimis, Geothechnical characterization of a thermal cracked marble, 7th International Congress on Rock Mechanics, Balkema, Rotterdam, 1991353–361.
34. A.R. Najibi, M. Ghafoori, G.R. Lashkaripour, M.R. Asef, Empirical relations between strength and static and dynamic elastic properties of Asmari and Sarvak limestones, two main oil reservoirs in Iran, J Pet Sci Eng 126 (2015) 78–82, https://doi.org/10.1016/j.petrol.2014.12.010.
35. V. Brotóns, R. Tomás, S. Ivorra, J.C. Alarcón, Temperature influence on the physical and mechanical properties of a porous rock: san Julian's calcarenite, Eng Geol 167 (2013) 117–127, https://doi.org/10.1016/j.enggeo.2013.10.012.
36. C. Inserra, S. Biwa, Y. Chen, Influence of thermal damage on linear and nonlinear acoustic properties of granite, Int J Rock Mech Min Sci 62 (2013) 96–104, https://doi.org/10.1016/j.ijrmms.2013.05.001.
37. P. Hartlieb, M. Toifl, F. Kuchar, R. Meisels, T. Antretter, Thermo-physical properties of selected hard rocks and their relation to microwave-assisted comminution, Miner Eng 91 (2016) 34–41, https://doi.org/10.1016/j.mineng.2015.11.008.